IEEE Access
Multidisciplinary | Rapid Review | Open Access Journal

Received July 27, 2020, accepted August 18, 2020, date of publication August 24, 2020, date of current version September 4, 2020.

Digital Object Identifier 10.1109/ACCESS.2020.3019083

Design and Automatic Fabrication of Novel Bio-Inspired Soft Smart Robotic Hands

YANG YANG[1,2], (Member, IEEE), YUNQUAN LI[2], (Member, IEEE), YONGHUA CHEN[2], (Member, IEEE), YINGTIAN LI[2,3], (Member, IEEE), TAO REN[4], AND YI REN[5]

[1]School of Automation, Nanjing University of Information Science and Technology, Nanjing 210044, China
[2]Department of Mechanical Engineering, The University of Hong Kong, Hong Kong
[3]Institute of Biomedical & Health Engineering, Shenzhen Institute of Advanced Technology, Chinese Academy of Sciences, Shenzhen 518055, China
[4]College of Nuclear Technology and Automation Engineering, Chengdu University of Technology, Chengdu 610059, China
[5]Robotics X Lab, Tencent, Shenzhen 518000, China

Corresponding authors: Yang Yang (meyang@nuist.edu.cn) and Yonghua Chen (yhchen@hku.hk)

This work was supported in part by the Startup Foundation for Introducing Talent of Nanjing University of Information Science and Technology (NUIST) under Project 1441092001001, and in part by the National Natural Science Foundation of China (NSFC) under Project 51805443.

ABSTRACT Soft material robots are developing rapidly benefited from their inherent flexibility, adaptability and safety compared to rigid-bodied robots. However, most soft robots are unable to offer high force/strength due to the low rigidity of soft materials that they are composed of. Absence of position feedback is another problem for soft robots. In this research, we aim to address these two challenges in a novel designed soft smart robotic hand. The design of this soft hand is also delicately considered to make it 3D printable, which shortens the design cycle and reduces the fabrication time. This hand consists of five fingers and a palm, all of which can be actuated independently. The finger is designed with two chambers: one air-tight active chamber which can be actuated by compressed air, one passive chamber filled with loosely arranged particles. During bending actuation, particles inside the passive chamber are squeezed by pressurized air, which causes passive jamming. As a result, the stiffness of the finger is strengthened during bending, which endows the hand with larger force output and load-holding capability. Furthermore, position feedback modules made of conductive elastomers are integrated and co-printed with the finger during fabrication. In this research, a hand prototype is manufactured and several experiments regarding to its characteristics and performance are conducted for evaluation. From experimental results, the soft hand achieves maximum holding weight of 1.452kg with particles and 0.8425kg without particles at same actuation pressure of 450kPa.

INDEX TERMS Soft robotics, variable stiffness, position feedback, passive jamming, granular materials.

I. INTRODUCTION

The research of anthropomorphic robotic hands is a significant area in robotics with possible applications in service robots where human-robot interaction is frequent, or in prosthetics for the handicapped to restore lost hand functions and so on [1]. Within the robotic hand group, soft robotic hands are gaining increasing interest from researchers owing to their inherent compliance when grasping objects of different nature, adaptability to unknown environments and safe interactions with humans compared to their rigid counterparts [2]–[4]. Therefore, developing anthropomorphic robotic hands with soft materials has been intensively investigated by researchers in recent years.

Deimel *et al.* proposed an under-actuated soft robotic hand consisting of seven soft pneumatic actuators [5]. Two of the actuators composed the palm and were used to achieve thumb opposition. Their study focused on investigating dexterous grasping of the hand. Yamaguchi *et al.* developed a soft robotic hand utilizing a kind of functional fluid-electro-conjugate fluid (ECF) for actuation of the fingers [6]. The ECF is able to produce a jet flow when high DC voltage is applied and thus leading to finger's bending deflection. In their research, they also attempted to realize flexion motion of palm by adding to the hand two bending units which are made of balloon actuators. One bending unit was designed

The associate editor coordinating the review of this manuscript and approving it for publication was Yingxiang Liu.

for thumb opposition while the other one was for metacarpal motion. Zhao *et al.* integrated stretchable and flexible optical waveguides into soft fingers [7]. The soft prosthetic hand was enabled with shape and texture detection benefited from the integrated optical sensors. The palm part of the hand was 3D printed with rigid material. A soft robotic hand proposed by Scharff *et al.* had ten air chambers in total for actuation including the wrist's movement [8]. The specialty of this work was that the whole hand was totally 3D printed (selective laser sintering, in particular) with flexible materials. Palm actuation was not included in their design. More recently, Zhou *et al.* proposed an anthropomorphic soft robotic hand with 26 independent degrees of freedom (DOFs) to replicate the human hand dexterous motions [9]. They have divided the palm into 4 sub-zones with 15 DOFs in total. While the hand can achieve lots of complicated postures, it also requires much fabrication and control effort.

From literature review, we noticed that the development of soft robotic hands mostly focused on fingers while palm designs are not specifically taken into consideration. Some palm designs merely function as support for grasping. As for those soft hands with independent palm design and actuation [5], [6], [9], the experimental results demonstrated that the palm actuation was helpful in providing effective and dexterous grasping. In this paper, we have designed the palm part for the hand separately. The palm structure is largely simplified from the real human hand but can still realize major bending (metacarpal motion) and secondary bending (instead of thumb opposition) to realize effective grasping.

A great challenge for soft robotics including soft hands is that they cannot offer high force/strength due to the low rigidity of the soft materials. An alternative to solve this problem is to enable the soft robots with variable stiffness capabilities. To be more specific, soft robots should possess low stiffness and high compliance in situations where flexibility and adaptation to environment are expected. Whereas, the robots have to be stiffened to be able to output high force or hold large load while maintaining their shape.

Variable stiffness methods adopted in soft robotics can be summarized into two categories: active and semi-active [10], [11]. Active methods refer to realizing variable stiffness by combining mechanisms with actuations, such as a combination of contracting and expanding McKibben actuators [12], a couple of DEA actuators with their pre-stress tuned by controlled activation [13] and fluidic actuators combined with tendons [14]. Different from active methods, semi-active methods utilize the modulation of material's intrinsic properties (such as elastic modulus or viscosity) to realize variable stiffness [15]. Materials that have been used for semi-active stiffness modulation include granular materials (jamming) [16], shape memory polymers [17], [18], low melting point alloys [19], low melting point polymers [20], eletro- and magneto-rheological fluids, etc. [21], [22]. Among these materials, jamming based granular materials have raised a lot of research interest in soft robotic field recently [23]–[25] benefitted from their large stiffness variation (50x [26]) and fast response speed. However, one drawback of granular jamming is that specific equipment to produce the jamming effect is usually essential, which is heavy, noisy and cumbersome. In this study, we have adopted a novel jamming method to overcome this drawback which will be further explained in following parts.

In this research, we propose a novel soft smart robotic hand which is inspired by human hands and is suitable for automatic fabrication. Soft robots' fast and automatic fabrication such as 3D printing has attracted researchers' interest in recent years [27]–[29]. 3D printing of soft robots has great significance in promoting their applications, shortening the development cycle, as well as making the robots accessible and affordable to every family.

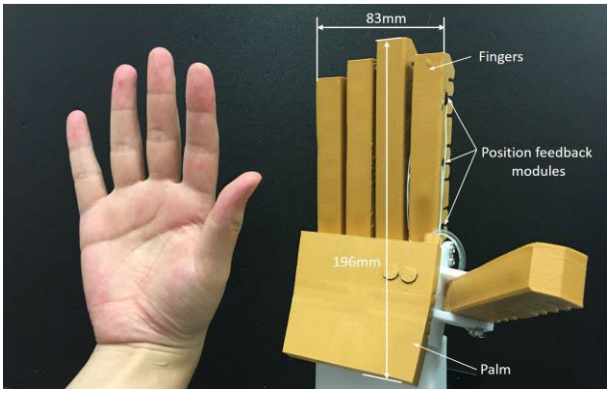

FIGURE 1. Comparison between the human hand (left) and the bio-inspired soft smart robotic hand (right).

By naming it as ''smart'', we refer to two aspects: 1) the hand is able to vary its stiffness upon grasping (stiffening in particular), thus making it possible to offer large lifting forces with small grasp forces; 2) the finger is enabled with position feedback which could be used for closed-loop control. The soft smart robotic hand proposed in this paper is shown in Fig.1 with comparison of a human hand. Variable stiffness of this hand is realized by jamming phenomenon of granular materials. While we have mentioned jamming when listing different intrinsic variable stiffness methods, the jamming method that is applied in this paper (which is passive granular jamming [30]) is different from most jamming methods. By passive jamming, the granules are confined and compressed by soft pneumatic actuators during actuation. In this way, jamming phenomenon is produced with only compressed air, making the jamming system get rid of vacuum pumps. Compared to previously proposed passive jamming method by the authors [30], further improvements made in this work are twofold. Firstly, the fabrication of soft pneumatic actuator is realized by 3D printing, which is faster and easier than molding of silicone rubber in previous research. Secondly, sheath for encasing granules is also 3D printed and integrated with the soft pneumatic actuator, thus making the fabrication of the whole finger completed in one 3D printing process. As for position feedback of the finger, it is implemented by embedding conductive

thermoplastic polyurethane (TPU) into the finger joints. Due to the piezo-resistive effect of conductive TPU, their resistance will change during the finger's bending and thus position feedback could be realized by measuring the resistance change. Moreover, conductive TPU are 3D printed concurrently with the finger's body without extra process to embed them.

The remainder of this paper is organized as follows. Section II explains the design principle of the novel soft hand and conducts finger stiffness modeling. The hand's configuration and its fabrication process are presented in Section III. In Section IV, several evaluation tests regarding to the hand's performance are conducted. Finally, Section V summarizes the paper and provides future work. Main contributions of this research include:

1) Novel design of a 3D printable bio-inspired soft hand;

2) Passive jamming to realize stiffening of the fingers during bending motion as well as better shape adaption without the need for vacuum pump;

3) Position feedback modules integrated into the finger which could potentially be used for close-loop control and developing sophisticated grasping strategy.

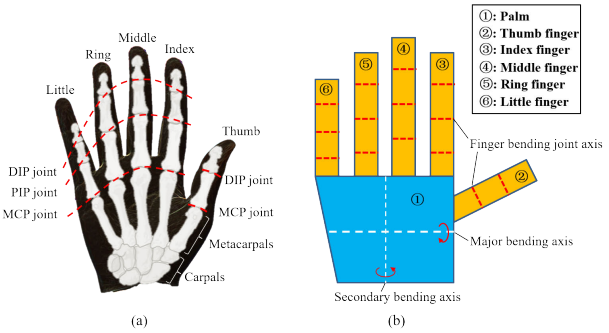

FIGURE 2. Design concept and bio-inspiration from human hand. (a) Bones and joints in human hand. (b) Components of the proposed soft hand.

II. DEVELOPMENT OF THE BIO-INSPIRED SOFT SMART ROBOTIC HAND

A. DESIGN PRINCIPLE

The nature has provided us a lot of inspirations for robot development [31]. Our human hands are very dexterous and can perform a large variety of tasks. From schematic diagram of human hand showing inner bones and joints in Fig.2(a) [32], the thumb has two bending joints while the other four fingers have three bending joints. Instead of merely a rigid support or platform, the palm is endowed with metacarpal motion and thumb opposition, making it an indispensable part for effective grasping. While in our proposed design in Fig.2(b), the five fingers numbered from ② to ⑥ are bio-inspired from the human finger's bending motion. Instead of continuous bending, the fingers are enabled with segmented bending and the bending axes are just the same as human hand. This segmented bending with joints also makes it possible to integrate sensing modules at finger joints for joint angle perception, thus realizing position feedback. For the palm numbered ①, it is designed with two degrees of freedom to mimic the flexion motion of human palm. In place of directly replicating human palm's structure, we aim to achieve the function of human hand and realize effective grasping by designing two bending axes. The main bending axis shown by thick dotted line mimics the metacarpal motion while the thumb opposition is replaced by secondary bending of the palm indicated by thin dotted line. It is expected that this bio-inspired hand design would offer a new sight into the development of soft robotic hand from biomimetic perspective.

B. PASSIVE GRANULAR JAMMING PRINCIPLE

Granular material system undergoes a jamming transition from liquid state to solid state when volume fraction of granules increases [33]. Most jamming systems applied in robotics use vacuum pump to change vacuum pressure and thus changing the volume fraction of the jamming system. Thus, vacuum pump is indispensable for vacuum-based jamming. For the gripper composed of soft pneumatic actuators, the compressed air not only actuates the gripper but also realizes the stiffening of the gripper. In this way, design and operation of the variable stiffness gripper is largely simplified with no extra operations needed for particle jamming. Here, we adopt a novel granular jamming method, i.e., passive granular jamming. The first version of passive granular jamming finger used an inextensible outer sheath to encase a soft expandable actuator molded by silicone rubber and a pack of granules [30]. Although passive jamming is achieved during actuation, the fabrication process is time consuming with multi-steps and not automatic. In this study, we propose an improved version of passive granular jamming finger benefited from 3D printing. The whole finger's structure is 3D printed with flexible material except for the granules which are filled inside after 3D printing. Profited from the automatic fabrication technique, fabrication process is largely simplified, and design cycle is shortened. Schematic explanation of the design principle for this new version of passive granular jamming finger is presented in Fig.3. It is obvious that the loosed particles/granules are squeezed and passively jammed when pressurized air fills inside the soft pneumatic actuator. As a consequence, the finger is stiffened during bending, enabling it with larger force output and larger load-holding capability.

C. FINGER DESIGN

Following the design principle and the passive jamming's working principle, the bio-inspired finger design is illustrated in Fig.4 (taking the index finger with three bending joints for instance). From the morphology of a human index finger shown in Fig.4(a), bending only occurs at three joints with crease while other regions with bones inside remain straight during the finger's bending. In our proposed finger model, the finger has two chambers: one air-tight active chamber which can be actuated by compressed air forming a

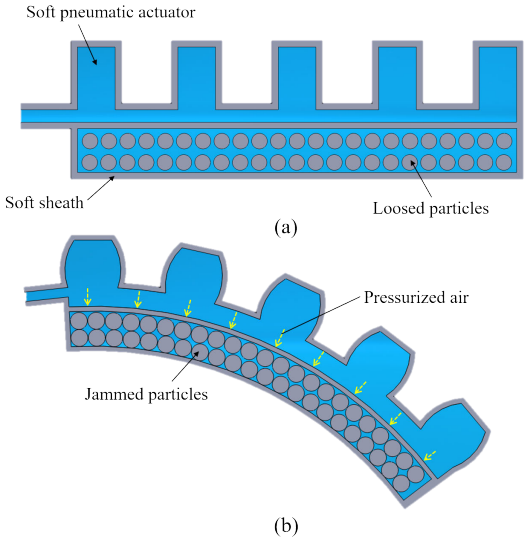

FIGURE 3. Passive jamming and stiffening of the finger during bending. (a) The actuator is at primary state and the particles are loosely arranged. (b) The actuator is deflected under pressurized air and particles encased in soft sheath are passively jammed, thus increasing the stiffness of the whole finger without use of vacuum pump.

pneumatic actuator and one passive chamber filled with loosely arranged particles as shown in Fig.4(b). Creased features are also introduced in the finger to induce bending at these regions when actuated, thus forming three bending joints. Other regions remain straight due to the thick structure. At the finger base, there are two holes for hand assembly and a slot for particle loading. To achieve positional feedback of the finger, feedback modules made of conductive TPU are integrated at the finger joints (below the creased features) as shown in Fig.4(c). Position feedback modules are connected to resistance meters for resistance measurement. The conductive TPU can also be processed by fused deposition modelling (FDM), thus making the whole finger 3D printable.

D. STIFFNESS MODELING

To predict the enhancement of finger stiffness benefited from the passive jamming, an analytical model is proposed here.

The geometrical modeling of the soft bending finger will be discussed first. As shown in Fig. 5, the finger only bends at three arcs $\hat{AB}$, $\hat{CD}$,and $\hat{EF}$ according to the mechanical design; the segments MA, BC, DE, NF remain straight. When the bending angle the soft finger equals to φ, the bending angle of each arc equals to $\varphi/3$. In the bending process, the length of $\hat{AB} = \hat{CD} = \hat{EF} = constant$, the radius of each arc changes with the change of the bending angle, therefore, we have $\hat{AB} = \frac{\varphi}{3}O_1A$, based on geometrical relationship, the radius OM' of the entire soft finger can be expressed as:

$$OM' = OM - MM' = \left(\hat{AB}/(\varphi/3) + BCsin(\varphi/3) + BC/tan(\varphi/2) + AM/tan(\varphi/2)\right) - MM' \quad (1)$$

The cross-section dimensions of the air chamber and particle chamber are also given on the left side of Fig. 5, the width of the chamber is w, depth of the air chamber is a, depth of the particle chamber is defined as d.

For a soft bending actuator, the rotational stiffness is a suitable parameter for characterization of its stiffness, which is defined as:

$$k = \frac{M}{\theta} \quad (2)$$

where M is the moment applied to the finger, and θ is the rotation angle. The moment M can be equivalent to applying an external force F by force arm length l_F, and the soft finger is pushed backwards for displacement d_F, the F, l_F and d_F can be measured more conveniently in practice (Fig. 6(a)). The torque can be expressed as $M = Fl_F$. The angle θ can be calculated based on the finger displacement d_F, force arm length l_F, bending angle of the finger φ, and the curvature radius of the bending finger ρ (or OM') (Fig. 6):

$$\theta = tan^{-1}\left(OMsin\varphi/(\rho\,(1 - cos\varphi) - d_F)\right) - \frac{\pi - \varphi}{2} \quad (3)$$

To balance the applied external moment M, the finger generates a resultant moment M_R. For a finger without the particles, M_R is generated merely by the pressure P. For a finger with particles, friction force among jammed particles will work as well to balance M. Therefore, under same pressure, the applied moment M required to rotate the finger for a rotation angle θ with particle jamming effect is larger than that without particles, which leads to a larger rotational stiffness.

The modeling process is referred to [30], but with some modifications. In [30], the particle jamming is designed to take effect only when the pressure reaches a certain pressure, in this research, particle jamming begins once the pressure increases as the particles are filled below the bending actuator. In the modeling process, we assume the weight of the particles can be ignored; another assumption is that when the pressure increases, the particles squeeze each other under external pressure P (P is the pressure relative to the standard one atmosphere), contract area of the pressure is assumed to be $A = \pi D^2/4$, where D is the diameter of each particle, therefore, the interaction force can be expressed as $F = AP = \pi D^2 P/4$.

We first study the force on a single particle, as shown in Fig. 6(b), each particle is surrounded by 6 particles around it. The friction coefficient is μ between particles, in the vertical direction, the value of friction is expressed as $f_N = \mu F_N$. Based on force transmissions between particles, the normal force can be calculated as $F_N = \sqrt{3}F_P/3$. The friction force can be expressed as: $f = \sqrt{3}\pi\mu_f D^2 P/12$. For each particle, there exists four friction forces acting on the reference point; therefore, the resultant work done by the friction of each particle can be expressed as $w_f = 4sin(\pi/6)f\Delta d_F = \sqrt{3}\pi\mu_f D^2 P\Delta d_F/6$, where Δd_F is the displacement of each particle. It is assumed that the displacement of each layer is same, therefore, $\Delta d_F = Dd_F/h$, where h is the height of the particle pack, therefore, for each particle, $w_f = \sqrt{3}\pi\mu_f D^3 P d_F/6h$.

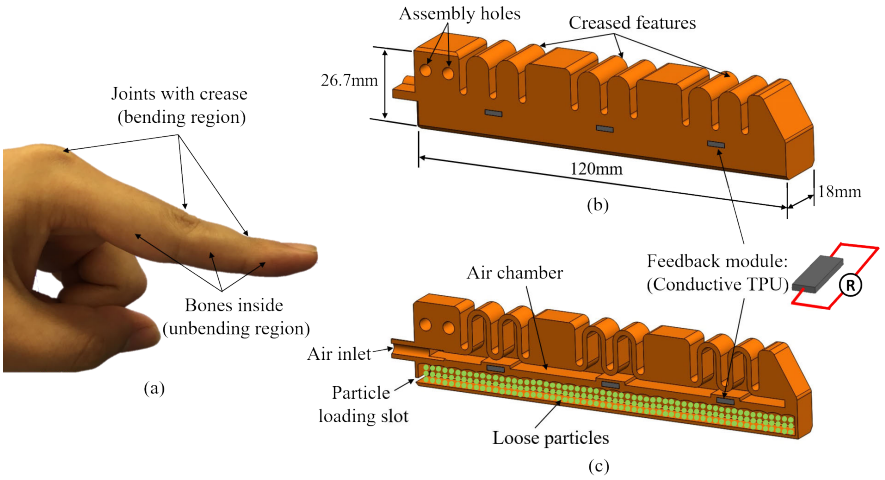

FIGURE 4. Bio-inspired finger design. (a) The morphology of human index finger. (b) 3D model of the proposed finger design with positional feedback (exterior appearance, dimensions are given for the proposed index finger model). (c): Cross-section view of the finger model.

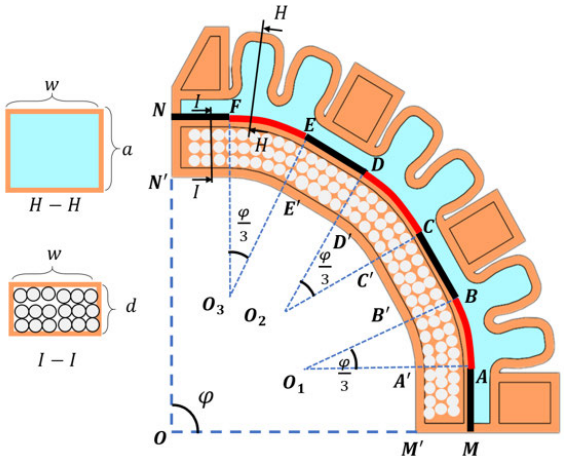

FIGURE 5. Geometrical modeling of the soft finger.

For each layer in X-Z plane (Fig. 6(a)), particle numbers can be calculated as $\boldsymbol{n = \sqrt{3}w(d - D)/3D^2}$, where w and d represent the width and depth of the particle chamber's cross-section (Fig. 5). The external work is consumed partly by the particles' friction. We assume there are m layers of particles ($\boldsymbol{m = h/D}$), the overall work done by the particles can be calculated as $\boldsymbol{W_f = \sum w_f = nmw_f = \pi \mu_f P d_F w(d - D)/6h}$. We assume that an equivalent resultant friction force $\boldsymbol{f_R}$ by particle jamming is acting in the middle of the gripper as shown in Fig. 6(a), the resultant friction force arm length can be obtained by $l_f = l_F/2$. The work can be expressed as $\boldsymbol{W_f = f_R d_F}$. Thus, the equivalent resultant friction force can be calculated as:

$$\boldsymbol{f_R = \frac{(\pi \mu_f P d_F w(d - D)/6)}{d_F} = \frac{\pi \mu_f P w(d - D)}{6}} \quad (4)$$

The bending torque generated by air pressure against the distal end of the finger can be calculated based on the method in [34]: $\boldsymbol{M_P = a^2 wP/2}$, where a and w are the height and width of the finger air chamber.

Therefore, considering that the toques at point M' are balanced, we have

$$\boldsymbol{M_F = M_P + M_f} \quad (5)$$

Therefore, the rotational stiffness can be expressed as:

$$\boldsymbol{k = \frac{M_F}{\theta} = \frac{M_P + M_f}{\theta} = \frac{a^2 wP/2 + f_R l_f}{\theta}} \quad (6)$$

That is:

$$\boldsymbol{k = \frac{a^2 wP/2 + \pi \mu_f l_f P w(d - D)/6}{tan^{-1}\left(OM sin\varphi'/(OM'(1 - cos\varphi) - d_F)\right) - (\pi - \varphi)/2}} \quad (7)$$

E. POSITION FEEDBACK PRINCIPLE AND APPLICATION

Position feedback of the soft material robots is currently challenging due to the absence of low cost, robust sensors that can be integrated in highly deformable structures without damaging their inherent compliance. What's more, the integration of commercially available sensors usually complicates the fabrication process [35]. Therefore, integrated sensor and actuator fabrication is highly desirable in soft actuator development. The finger design with position feedback modules is given in Fig.4(c), here we will explain the principle of the finger's position feedback in detail.

As a smart material, conductive TPU has piezoresistive effect which endows itself with resistivity change when stress is applied. The applied stress changes the volume fraction or concentration of conductive fillers inside conductive TPU. The variation trend of conductive elastomers' volume resistivity with incorporated carbon black (CB)'s concentration is presented in Fig.7(a) [36], [37]. During bending deformation, the position feedback module is under compression (located within compression region below the midline) as presented in Fig.7(b). The deformation of position feedback module leads to the change of CB's volume fraction, thus changing

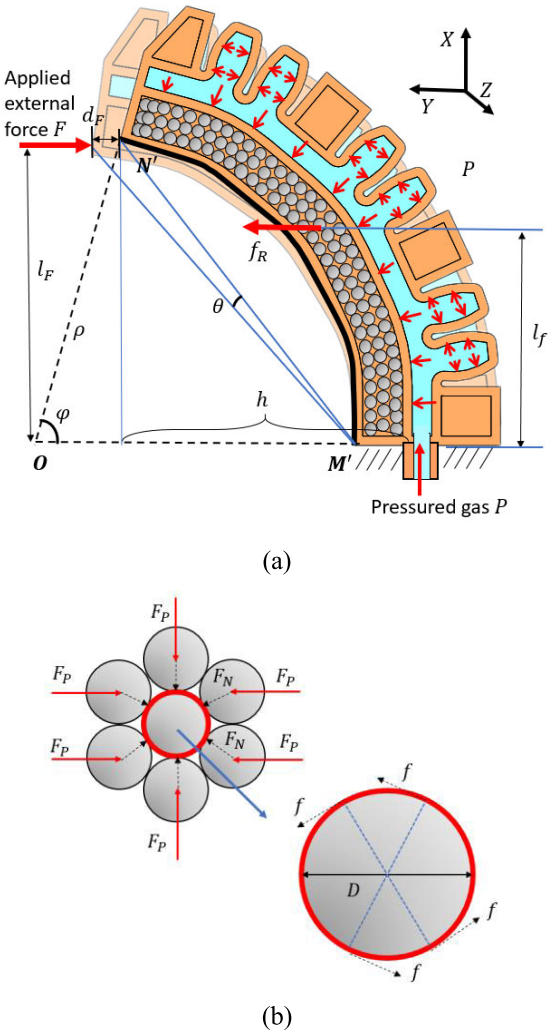

FIGURE 6. Modeling of the rotational stiffness of the soft finger (a) Applying an external force F at the finger. (b) Force analysis of the friction among particles due to particle jamming.

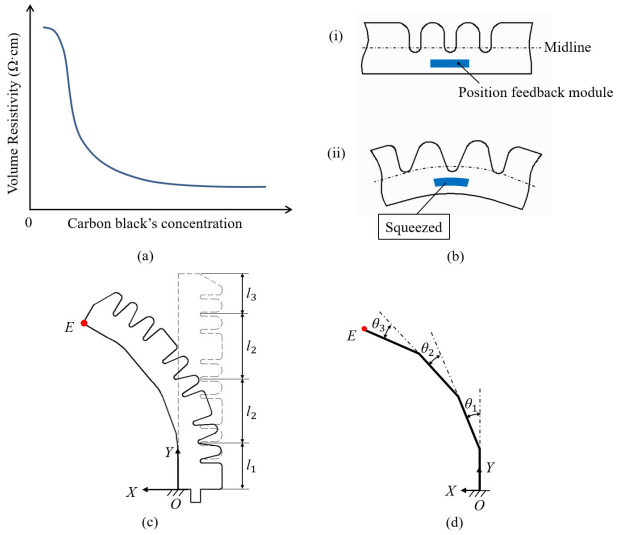

FIGURE 7. Principle of the finger's position feedback. (a) Relationship between resistivity and carbon black's concentration of conductive TPU. (b) Deformation of position feedback module at the finger joint. (c) Finger's bending deformation and dimensional parameters. (d) Finger kinematics.

the resistance of position feedback module [38]. By characterization of the position feedback module, we can obtain the relationship between the joint bending angle and the feedback module's resistance change. Fig.7(c) shows the deformation of the whole finger during bending and the finger's kinematics is shown in Fig.7(d), simplified as four rods connected by three rotational joints. The rotation angles of the three joints are indicated as θ_1, θ_2 and θ_3. The base coordinate is labeled as X-Y in Fig.7(c) and Fig.7(d), with the fingertip point 'E' set as the reference point for position feedback. Based on the kinematics, coordinate of 'E' (x, y) is calculated by:

$$\begin{cases} x = l_2\,(sin\theta_1 + sin(\theta_1+\theta_2)) + l_3 \sin\,(\theta_1+\theta_2+\theta_3) \\ y = l_1 + l_2\,(cos\theta_1 + cos(\theta_1+\theta_2)) + l_3 cos\,(\theta_1+\theta_2+\theta_3) \end{cases} \tag{8}$$

where l_1, l_2 and l_3 are the length of the rods (different segments of the finger are directly related to the finger's geometrical dimension). Once θ_i $(i = 1, 2, 3)$ is obtained by measuring the resistance change of position feedback modules, coordinate of the fingertip point 'E' can be derived with (8) when referring to the characterization results. As a consequence, position feedback is realized.

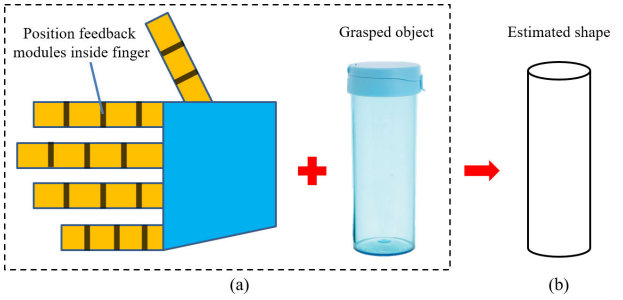

FIGURE 8. Estimation of grasped object's shape and size with position feedback for the hand's fingers. (a) Grasping with position feedback information. (b) Estimated shape of grasped object.

Once the fingers are endowed with position feedback, the hand can be applied to estimate the shape and size of the grasped object. The estimation sketch is shown in Fig.8. Due to the inherent compliance of the soft hand, the fingers and the palm can adapt themselves to the object's shape upon grasping. By detecting the resistance change of feedback modules, the fingers' position is derived. Therefore, the external profile of the grasped object containing its shape and size information can be estimated. In future, tactile sensors will also be integrated into the hand to provide more precise feedback information.

F. PALM DESIGN

As stated in Section II-A, the palm also plays an important role during hand manipulation. To design a palm part with two axes of bending motion which are actuated by pressurized air simultaneously, internal chamber of the palm has to be delicately designed. 3D model of the proposed palm design is presented in Fig.9. Fig.9(a) shows the exterior appearance

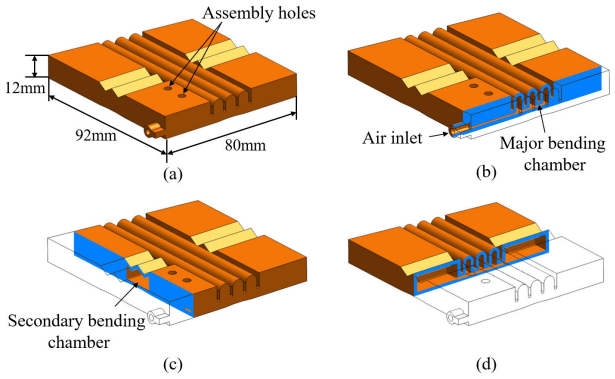

FIGURE 9. Bio-inspired palm design. (a) 3D model of the proposed palm design. (b) Cross-section view showing shape of the air chamber that leads to major bending. (c) Cross-section view showing shape of the air chamber that leads to secondary bending. (d) Cross-section view showing the connection between major bending chamber and secondary bending chamber.

of the palm model while Fig.9(b) to (d) show the internal structure of the palm by giving cross section views at different sections. It can be seen that the major bending axis is realized by creased feature just like the finger joints while the secondary bending axis is also enabled with creased feature but with shorter length and a smaller number of creases. Chambers for major bending and secondary bending are connected, making it possible to actuate the two axes of bending motion at the mean time when pressurized air is filled through the air inlet.

III. HAND FABRICATION

A. HAND CONFIGURATION

The soft hand consists of five fingers and a palm which can all be actuated independently. To assemble the fingers and the palm, 3D printed support parts are designed to locate and fix the fingers and palm by connection holes and screws. The support parts are also designed leaving out space for air pipes from the fingers and palm to connect with control valves and air source. 3D model of the hand configuration can be seen in Fig.10. Different length of the fingers is inspired by the human hand configuration. The palm and thumb are placed in inclined planes to achieve better grasping. After assembly, the hand can be planted on a robotic arm to perform tasks or on a platform for testing. In this study, we only integrate position feedback modules on the index finger to test the design proposal of the soft smart hand. All fingers will be endowed with position feedback in future study.

B. FABRICATION

To achieve automatic fabrication of the soft hand, the fingers and the palm are all manufactured by 3D printing, in particular the fused deposition modelling (FDM). Flexible material composing the palm and the main body of the fingers is NinjaFlex (NinjaTek, USA), which is a thermoplastic elastomer filament. For the conductive material to fabricate position feedback parts, Palmiga-PI-ETPU 95-250 (Palmiga Innovation AB, Sweden) is used. It is a compound of thermoplastic

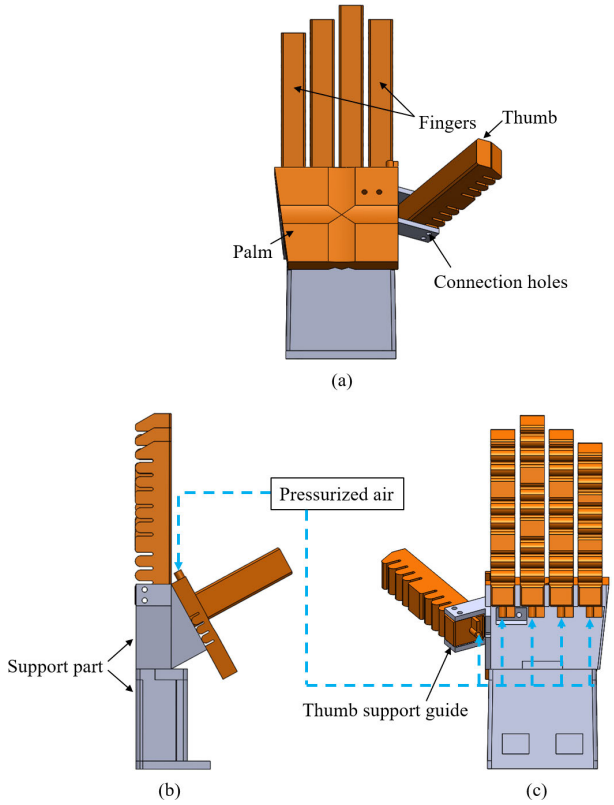

FIGURE 10. Hand configuration. (a) Palmar view of the hand model. (b) Lateral view of the hand model. (c) Back view of the hand model.

polyurethane and carbon black fillers. Both of the two materials can be processed by FDM printer, thus making the fingers and palm 3D printable. Main properties of these materials are listed in Table 1.

TABLE 1. Properties of the materials for 3D printing.

Properties	Materials	
	Palmiga-PI-ETPU 95-250 [39]	NinjaFlex [40]
Density/g·cm^{-3}	1.3	1.19
Tensile strength (Yield) /MPa	15	4
Tensile modulus /MPa	12	12
Volume resistivity/Ω·cm	<100	NA
Hardness	Shore 95 A	Shore 85A

Although the palm can be 3D printed with single head FDM 3D printer, fingers with positional feedback have to be fabricated using a dual-head 3D printer since it is composed of multiple materials. A dual head FDM printer Makerbot Replicator 2X (Makerbot Inc., USA) is used to print the finger position feedback modules. For the palm merely composed of flexible material, it is fabricated with a single head FDM printer QIDI Tech I (Qidi Technology Co., China). The palm can also be printed with the dual head printer. Here we use another printer to speed up the fabrication process. Supporting materials are not used during the 3D printing process to guarantee the quality of the inner air chambers.

The overhanging parts (small overhang only) can be printed without support due to the high elasticity of the flexible filament. The feasibility for 3D printing is also taken into consideration during finger and palm model design. Parameters regarding to the dual-material 3D printing process is listed in Table 2. Details on the precautions of printing airtight parts with flexible filament NinjaFlex on a FDM machine can be found in reference [41]. For 3D printing with conductive TPU, the carbon black fillers may block the nozzle after a period of fabrication. Therefore, it is helpful to clean the nozzle with other printing materials such as polylactide (PLA) to prevent this disadvantage.

TABLE 2. Dual-material 3D printing settings.

Parameters	Values
Extruder temperature for Conductive TPU (℃)	220
Extruder temperature for NinjaFlex (℃)	245
Build plate temperature (℃)	40
Nozzle size (mm)	0.4
Layer thickness (mm)	0.1
Shell thickness (mm)	1.6
Print speed (mm/s)	30

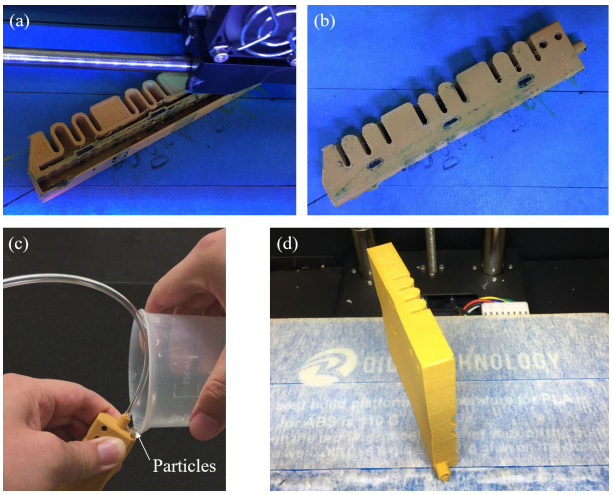

FIGURE 11. Fabrication process. (a) Snapshot of the finger's 3D printing process. (b) Fabricated finger on the built platform. (c) Loading the finger with particles. (d) 3D printed palm.

Fig.11(a) and (b) show the printing process of the fingers with position feedback modules. The black parts are printed in Conductive TPU and the mustard color parts are printed in NinjaFlex flexible material. When high stiffness of the hand is required, particles can be filled inside the passive chamber of the finger through a slot (Fig.11(c)) and then sealed with hot melt adhesive. 3D printing of the palm is shown in Fig.11(d) and the printing direction ensures that the overhanging part of the palm is very small. Variation of the colors in Fig.11 is mainly attributed to the lighting environment.

IV. EXPERIMENTAL STUDY

A. HAND MOTION

After fabrication and assembly, the hand is ready for different tests. First, hand motion is tested to examine the fundamental

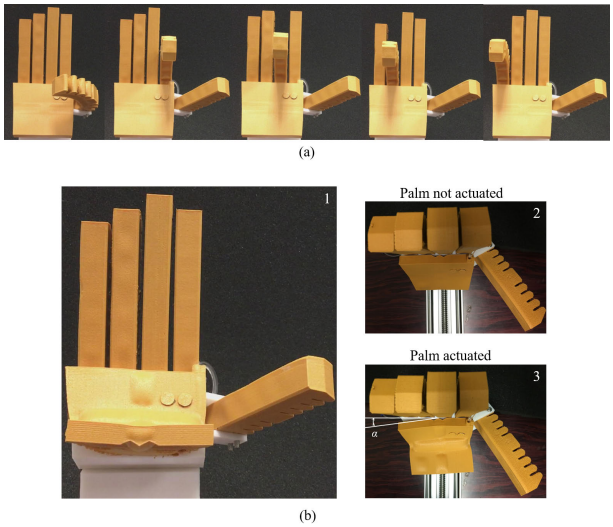

FIGURE 12. Hand motion. (a) Finger motions: the fingers are actuated from left to right in the following order: thumb, index, middle, ring and little finger. (b) Palm motion: palmar view (1), top view (2 and 3).

functions of the hand. During hand motion test, particles are not embedded inside the fingers. Fig.12(a) demonstrates the motions of five fingers in turn and Fig.12(b) demonstrates the palm's motion. From palmar view in Fig.12(b)(1), the metacarpal motion realized by major bending chamber is obvious. The palm's secondary bending motion can be seen by comparison between Fig.12(b)(2) and Fig.12(b)(3). The palm has a bending angle indicated by α from top view. This secondary bending motion replaces thumb opposition and contributes to effective and firm grasping. During hand motion test, the actuation air pressure for five fingers is 400kPa and the pressure for the palm is 200kPa. The air pressures are controlled by pressure control valves (AR20-01-A, SMC Corporation).

B. FINGER STIFFNESS AND CURVATURE TE

To examine the stiffening effect by introducing particles inside the finger, finger stiffness test is conducted. Moreover, the passive chamber filled with particles has an effect on the finger's curvature during bending, which should also be experimentally investigated.

The stiffness of a structure is defined as the ability of this structure to hold its own shape when external load is applied. In this test, the applied load is a rotation moment induced by the external force and corresponding deformation expressed by the rotation angle of the finger is measured. Rotational stiffness of the finger is given in (6).

The stiffness test sketch is shown in Fig.13(a) and the real test set-up is shown in Fig.13(b). The ring finger is chosen for test here and the test result can be referred by other fingers.

Stiffness measurement is conducted as follows. Firstly, the finger is actuated with a pre-set air pressure and stabilized to a certain position (l can be measured). Air pressure of the finger is controlled by an electro-pneumatic regulator (SMC ITV2030-212L, output 0.005∼0.5MPa). Then the

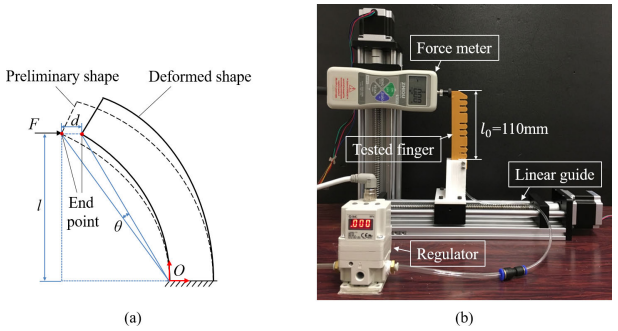

FIGURE 13. Stiffness test principle and set-up. (a) Measurement of the ring finger's rotational stiffness. (b) Real set-up.

force meter (range: 0∼100N, precision: 0.01N) is leveled to make sure the center of its probe is just in touch with the finger's end point. Following this, step motor driven linear guide pushes the finger toward the force meter for a distance of d (d = 5mm in this test) and the force meter records applied force on the finger in real time. Average value of the recorded force data is denoted as F. θ can be calculated when the finger bends to a certain position and d is known. During the test, air pressure of the finger increases from 0 to 450kPa with an interval of 50kPa. At each pressure, measurement of the applied force F is repeated 10 times and then the average value and standard deviation is calculated. Using equation (6), rotational stiffness of the finger k is obtained.

The test result is presented in Fig.14(a). It is obviously that the finger's rotational stiffness is strengthened with particles inside the passive chamber. Also, the stiffening effect becomes better as the actuation pressure increases. This is reasonable since the squeeze and jamming of particles are more sufficient at a larger actuation pressure. The finger achieves a rotational stiffness of 2621N·mm/rad with particles and 1223 N·mm/rad without particles at 450kPa. The former value is 2.14 times of the latter one.

Before the proposed finger can be practically applied, test regarding to particles' effect on the finger's curvature is essential. In the finger curvature test, radius of the finger is recorded using a HD camera. Air pressure of the finger also increases from 0 to 450kPa with 50kPa's interval as the stiffness test. At each pressure, the finger's radius of curvature with and without particles is measured. The test result in Fig.14(b) demonstrates that finger with particles inside has a larger radius of curvature compared with finger without particles under same applied pressure. This means that introducing particles inside the finger affects the finger's curvature to some extent. However, this effect becomes smaller as the air pressure increases. Therefore, the particles' effect on the finger's bending curvature is negligible when applied on soft hand at an actuation pressure of around 400kPa.

To validate the effectiveness of the theoretical modeling, we calculate the analytical values of finger stiffness based on the modeling conducted in Section II-D. Parameters regarding to the modeling: a = 15mm, w = 16mm, μ_f = 2.5, d = 10mm, D = 3mm, d_f = 5mm, OM'= ρ is the curvature

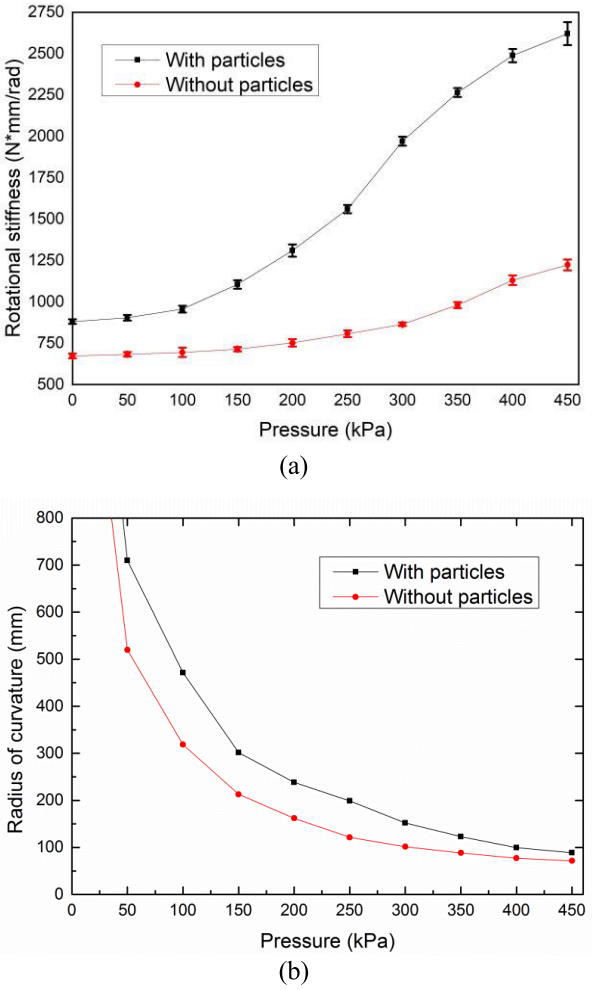

FIGURE 14. Test result. (a) Finger stiffness test result. (b) Finger's radius of curvature vs pressure.

radius of finger and is obtained from the experimental result in Fig. 14(b), l_f, h and φ are obtained from ρ based on the geometrical relationships shown in Fig. 6. The comparison result is shown in Fig. 15. It can be seen that the experimental result and theoretical result of finger stiffness have the same variation trend. The difference is caused by the test errors and the simplified assumptions during modeling.

C. FINGER POSTION FEEDBACK CHARACTERIZATION

1) RELATIONSHIP BETWEEN RESISTANCE AND JOINT BENDING ANGLE

The position feedback modules must be calibrated before conducting the finger's position feedback test. The test set-up for position feedback modules' calibration is shown in Fig.16. For the calibration test, the index finger is attached with markers for measurement of three joint bending angles. Although position feedback modules for three joints are in same dimension, their characteristics may be different after fabrication and connecting to wires. Therefore, it is necessary to calibrate each module separately. During the test, the finger's bending is controlled by a pneumatic regulator and the bending angles

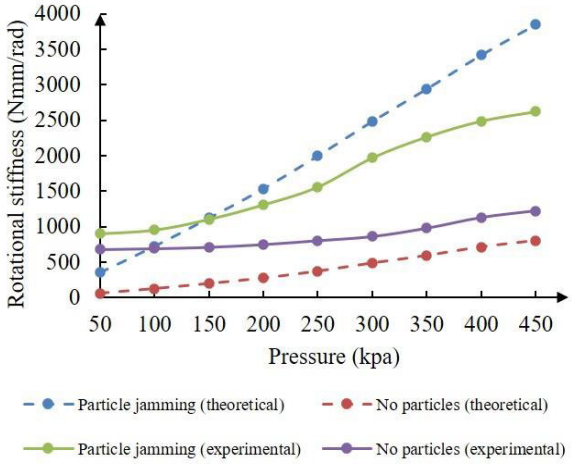

FIGURE 15. Finger stiffness experimental result vs theoretical result.

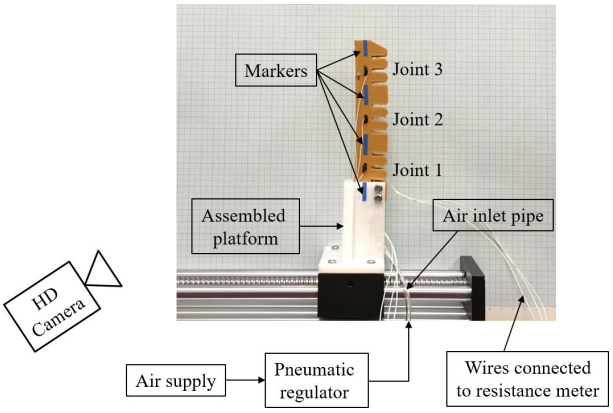

FIGURE 16. Position feedback module calibration set-up.

for three joints are recorded by a HD camera. Resistance of the position feedback modules are measured by digital resistance meters (Victor 86D) in real time.

Relationship of resistance change ΔR in the position feedback module to the corresponding joint's bending angle θ for all three joints is plotted in Fig.17. It can be seen that the characteristics of each feedback module is unique. Since the relationship shows nonlinearity, quadratic polynomial fit is performed for each feedback module to approximate the curve of ΔR-θ relationship.

The approximation results are listed as follows:

$$\begin{aligned}
\text{Joint } 1 &: \theta_1 = -0.2768 + 18.9962\Delta R + 16.3554\Delta R^2, \\
\text{Joint } 2 &: \theta_2 = 0.398 + 24.6585\Delta R + 34.0048\Delta R^2, \\
\text{Joint } 3 &: \theta_3 = -0.0132 + 27.6487\Delta R - 1.0714\Delta R^2, \quad (9)
\end{aligned}$$

With (8) and (9), position of the fingertip can be derived once resistance change of three position feedback modules is measured.

2) POSITION FEEDBACK TEST

Using calibration results, position feedback performance of the finger is evaluated in this test. Experimental set-up for position feedback test is shown in Fig.18. The tested finger's

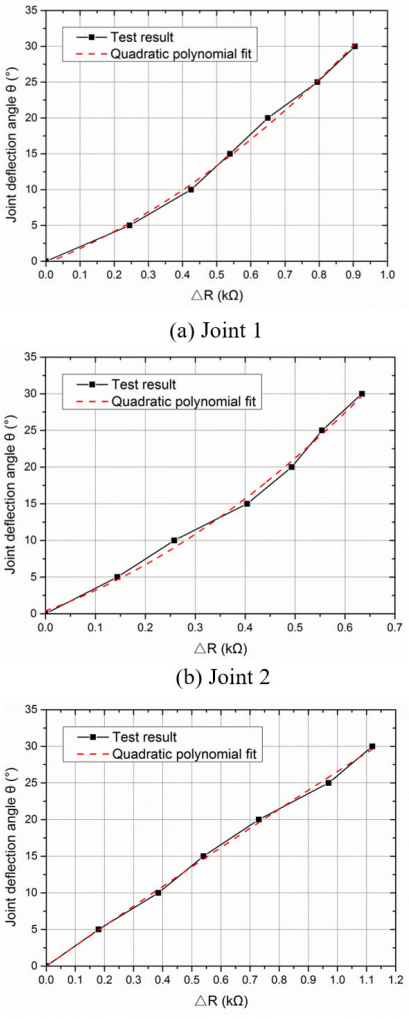

FIGURE 17. Calibration test results for three joints. (a) Joint 1. (b) Joint 2. (c) Joint 3.

bending motion is controlled using a pressure control valve and the fingertip's position is traced by camera. Resistance measurement of the position feedback modules is implemented with a simple circuit board. During measurement, each position feedback module is cascaded with a standard resistor (which resistance is given) with 5V voltage. Then the resistance of the feedback module is obtained simply by measuring the voltage on it. This is controlled using Arduino Nano and an analog-to-digital (A/D) converter (type: ADS1256, 24-bit) is adopted to transmit the data to computer. With the obtained resistance data, position of the fingertip (trace point) can be predicted and compared with visual measurement result considering (1) and (3).

Comparison result between visual measurement and positional feedback of the trace point is shown in Fig.19. During the test, air pressure of the finger increases from 0 to 400kPa with an interval of 80kPa. The six data points in Fig.19 are obtained at 0, 80kPa, 160kPa, 240kPa, 320kPa and 400kPa from right to left. It can be seen that the red circles and dotted line of position feedback result can basically reflect the real

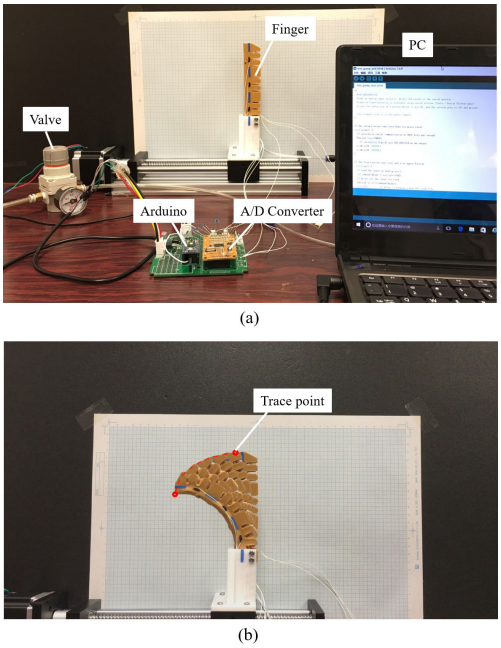

FIGURE 18. Position feedback test set-up. (a) The real set-up. (b) Visual measurement of finger trace point's trajectory.

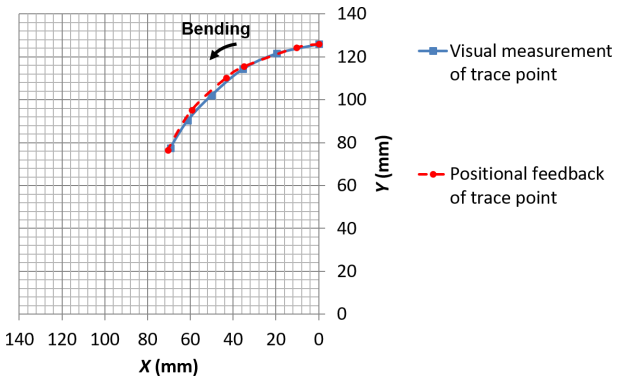

FIGURE 19. Comparison between visual measurement and positional feedback of trace point.

position of the finger which is in blue squares and solid line. Therefore, it is promising to realize position feedback of the soft fingers or actuators with this method. The difference between position feedback result and visual measurement may be caused by environmental disturbance as well as errors in calibration tests.

D. HAND HOLDING TEST

The stiffening effect of the introduced particles inside the finger is obvious from the finger stiffness test result. However, the effect of the whole hand's performance with all fingers filled with particles is still unknown. To evaluate the hand's performance with particles, hand holding test is performed. In this test, the hand is arranged at horizontal posture to hold an object against gravity. The hand holding test sketch is shown in Fig.20. The grasped object is designed with several raised features and is 3D printed. The raised features aim to realize better shape adaptation of particles. When the particles inside the fingers are at fluid state and not jammed, the particles can flow and easily adapt their shape to that of the grasped object. Once jammed, the hand can provide larger holding ability.

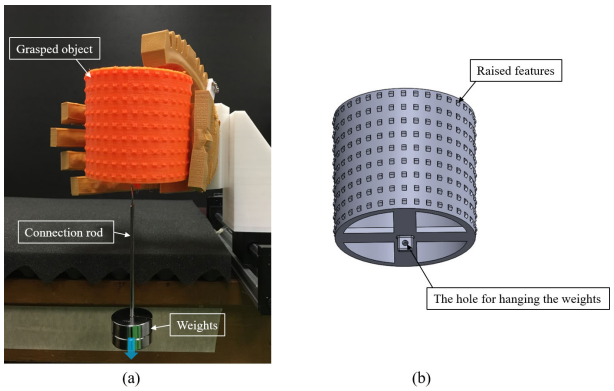

FIGURE 20. Hand holding test design. (a) Real test set-up. (b) Grasped object with raised features.

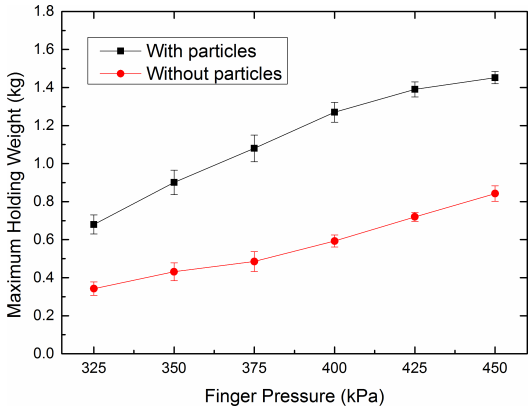

FIGURE 21. Hand holding test result.

In this test, air pressure of the palm keeps constant at 200kPa while the fingers begin with 325kPa and increases to 450kPa with 25kPa's interval. The starting pressure is 325kPa because curvature of the fingers is not enough to hold the grasped object at a smaller pressure. At each given finger pressure, grasp failure test is conducted by slowing adding weights hanged by the grasped object until the object is dropped. Each test is repeated five times and the average value of the maximal holding weight as well as standard deviation is calculated. Comparative experiment is also conducted on the hand when no particles are filled inside the fingers.

The test result is shown in Fig.21. We can see that the maximum holding weight of the hand increases as finger pressure increases both with and without particles. This is reasonable since the increased air pressure leads to larger contact force between the fingers and the object. It is worth noticed that the particles have obviously improved the hand's holding capability at the same finger pressure. At 450kPa, the hand's maximum holding weight is 1.452kg with particles and 0.8425kg without particles. From our proposed design, the hand is enabled to generate large lifting forces with

FIGURE 22. Grasping capability demonstration with various objects. (a) Grasping a baseball with thumb and index fingers. (b) Grasping an orange with thumb, index and middle fingers. (c) Grasping a box with thumb, index and middle fingers. (d) Grasping a metal bottle with thumb, index and the palm. (e) Grasping a wallet with thumb, index, middle and the palm. (f) Grasping a cellphone. (g) Grasping a plastic box packed with eggs. (h) Grasping a loudspeaker. (i) Grasping a roll of copper tape with all five fingers and the palm. (j) Grasping a digital multi-meter. (k) Grasping a champagne bottle.

small grasp forces benefited from the interlocking between deformed finger sheath filled with particles and the grasped objects.

E. GRASPING DEMONSTRATION

To demonstrate the versatility of the soft hand, grasping of a variety of objects with different geometrical shape and nature are performed, which are shown in Fig.22. As we have mentioned, particles inside the finger are not only aimed for passive granular jamming. The particles can also realize shape adaptation to objects with different shapes. Moreover, particles inside the fingers have damping and shock absorption effect, which can protect fragile objects from being damaged during shock [42]. A video showing the hand grasping different objects has been submitted together with this paper.

V. CONCLUSION AND FUTURE WORK

In this study, we have proposed a novel design of soft hand with smart properties. This novel design aims to settle two challenges in soft robotics: 1) inability to offer high force/strength due to the highly deformable and low-rigidity materials; 2) lack of effective sensing capabilities. In our proposed soft hand, soft pneumatic fingers are designed with passive chambers filled with particles inside. These passively jammed particles can stiffen the fingers during bending motion. 3D printed sensing parts are also integrated into the finger to provide position feedback. Moreover, a palm with two bending degrees is designed for effective hand grasping. The whole hand structure including the sensing modules is automatically fabricated benefited from 3D printing. Theoretical modeling of the finger stiffness is conducted and verified by the experimental results. Experiments regarding to the hand's smart properties and grasping performance are performed.

The position feedback modules integrated into the soft hand provide us with potential for conducting close-loop control and sophisticated grasping strategy on this proposed soft hand. In future study, we will integrate sensing modules to all the fingers and the palm for the shape detection of the grasped object and the automatic control. Theoretical models for the passive jamming phenomenon in the finger will also be investigated to optimize the hand performance.

REFERENCES

[1] J. T. Belter, J. L. Segil, A. M. Dollar, and R. F. Weir, "Mechanical design and performance specifications of anthropomorphic prosthetic hands: A review," *J. Rehabil. Res. Develop.*, vol. 50, no. 5, p. 599, 2013.

[2] L. Wang, S. G. Nurzaman, and F. Iida, "Soft-material robotics," *Found. Trends Robot.*, vol. 5, no. 3, pp. 191–259, 2017.

[3] C. Majidi, "Soft robotics: A Perspective—Current trends and prospects for the future," *Soft Robot.*, vol. 1, no. 1, pp. 5–11, Mar. 2014.

[4] J. Shintake, V. Cacucciolo, D. Floreano, and H. Shea, "Soft robotic grippers," *Adv. Mater.*, vol. 30, no. 29, 2018, p. 1707035.

[5] R. Deimel and O. Brock, "A novel type of compliant and underactuated robotic hand for dexterous grasping," *Int. J. Robot. Res.*, vol. 35, nos. 1–3, pp. 161–185, Jan. 2016.

[6] A. Yamaguchi, K. Takemura, S. Yokota, and K. Edamura, "A robot hand using electro-conjugate fluid: Grasping experiment with balloon actuators inducing a palm motion of robot hand," *Sens. Actuators A, Phys.*, vol. 174, pp. 181–188, Feb. 2012.

[7] H. Zhao, K. O'Brien, S. Li, and R. F. Shepherd, "Optoelectronically innervated soft prosthetic hand via stretchable optical waveguides," *Sci. Robot.*, vol. 1, no. 1, Dec. 2016, Art. no. eaai7529.

[8] R. B. Scharff, E. L. Doubrovski, W. A. Poelman, P. P. Jonker, C. C. Wang, and J. M. Geraedts, "Towards behavior design of a 3D-printed soft robotic hand," in *Soft Robotics: Trends, Applications and Challenges*. Cham, Switzerland: Springer, 2017, pp. 23–29.

[9] J. Zhou, X. Chen, U. Chang, J.-T. Lu, C. C. Y. Leung, Y. Chen, Y. Hu, and Z. Wang, "A soft-robotic approach to anthropomorphic robotic hand dexterity," *IEEE Access*, vol. 7, pp. 101483–101495, 2019.

[10] M. Manti, V. Cacucciolo, and M. Cianchetti, "Stiffening in soft robotics: A review of the state of the art," *IEEE Robot. Autom. Mag.*, vol. 23, no. 3, pp. 93–106, Sep. 2016.

[11] R. D. Kornbluh, H. Prahlad, R. Pelrine, S. Stanford, M. A. Rosenthal, and P. A. von Guggenberg, "Rubber to rigid, clamped to undamped: Toward composite materials with wide-range controllable stiffness and damping," *Proc. SPIE*, vol. 5388, pp. 372–386, Jul. 2004.

[12] K. Suzumori, S. Wakimoto, K. Miyoshi, and K. Iwata, "Long bending rubber mechanism combined contracting and extending tluidic actuators," in *Proc. IEEE/RSJ Int. Conf. Intell. Robots Syst.*, Nov. 2013, pp. 4454–4459.

[13] R. Pelrine, F. Carpi, D. De Rossi, R. Kornbluh, R. Pelrine, and P. Sommer-Larsen, "Variable stiffness mode: Devices and applications," in *Dielectric Elastomers as Electromechanical Transducers: Fundamentals, Materials, Devices, Models and Applications of an Emerging Electroactive Polymer Technology*. Oxford, U.K.: Elsevier, 2008, pp. 141–145.

[14] W. McMahan, B. A. Jones, and I. D. Walker, "Design and implementation of a multi-section continuum robot: Air-octor," in *Proc. IEEE/RSJ Int. Conf. Intell. Robots Syst.(IROS)*, 2005, pp. 2578–2585.

[15] L. Wang, Y. Yang, Y. Chen, C. Majidi, F. Iida, E. Askounis, and Q. Pei, "Controllable and reversible tuning of material rigidity for robot applications," *Mater. Today*, vol. 21, no. 5, pp. 563–576, Jun. 2018.

[16] E. Brown, N. Rodenberg, J. Amend, A. Mozeika, E. Steltz, M. R. Zakin, H. Lipson, and H. M. Jaeger, "Universal robotic gripper based on the jamming of granular material," *Proc. Nat. Acad. Sci. USA*, vol. 107, no. 44, pp. 18809–18814, Nov. 2010.

[17] Y. Yang, Y. Chen, Y. Li, M. Z. Q. Chen, and Y. Wei, "Bioinspired robotic fingers based on pneumatic actuator and 3D printing of smart material," *Soft Robot.*, vol. 4, no. 2, pp. 147–162, Jun. 2017.

[18] A. Firouzeh and J. Paik, "An under-actuated origami gripper with adjustable stiffness joints for multiple grasp modes," *Smart Mater. Struct.*, vol. 26, no. 5, May 2017, Art. no. 055035.

[19] B. E. Schubert and D. Floreano, "Variable stiffness material based on rigid low-melting-point-alloy microstructures embedded in soft poly (dimethylsiloxane)(PDMS)," *Rsc Adv.*, vol. 3, no. 46, pp. 24671–24679, 2013.
[20] M. A. McEvoy and N. Correll, "Thermoplastic variable stiffness composites with embedded, networked sensing, actuation, and control," *J. Compos. Mater.*, vol. 49, no. 15, pp. 1799–1808, Jun. 2015.
[21] A. Tonazzini, A. Sadeghi, and B. Mazzolai, "Electrorheological valves for flexible fluidic actuators," *Soft Robot.*, vol. 3, no. 1, pp. 34–41, Mar. 2016.
[22] C. Majidi and R. J. Wood, "Tunable elastic stiffness with microconfined magnetorheological domains at low magnetic field," *Appl. Phys. Lett.*, vol. 97, no. 16, Oct. 2010, Art. no. 164104.
[23] M. Cianchetti, T. Ranzani, G. Gerboni, T. Nanayakkara, K. Althoefer, P. Dasgupta, and A. Menciassi, "Soft robotics technologies to address shortcomings in Today's minimally invasive surgery: The STIFF-FLOP approach," *Soft Robot.*, vol. 1, no. 2, pp. 122–131, Jun. 2014.
[24] Y. Wei, Y. Chen, T. Ren, Q. Chen, C. Yan, Y. Yang, and Y. Li, "A novel, variable stiffness robotic gripper based on integrated soft actuating and particle jamming," *Soft Robot.*, vol. 3, no. 3, pp. 134–143, Sep. 2016.
[25] N. Cheng, J. Amend, T. Farrell, D. Latour, C. Martinez, J. Johansson, A. McNicoll, M. Wartenberg, S. Naseef, W. Hanson, and W. Culley, "Prosthetic jamming terminal device: A case study of untethered soft robotics," *Soft Robot.*, vol. 3, no. 4, pp. 205–212, Dec. 2016.
[26] A. G. Athanassiadis, M. Z. Miskin, P. Kaplan, N. Rodenberg, S. H. Lee, J. Merritt, E. Brown, J. Amend, H. Lipson, and H. M. Jaeger, "Particle shape effects on the stress response of granular packings," *Soft Matter*, vol. 10, no. 1, pp. 48–59, 2014.
[27] T. J. Wallin, J. Pikul, and R. F. Shepherd, "3D printing of soft robotic systems," *Nature Rev. Mater.*, vol. 3, no. 6, pp. 84–100, Jun. 2018.
[28] A. Zolfagharian, A. Z. Kouzani, S. Y. Khoo, A. A. A. Moghadam, I. Gibson, and A. Kaynak, "Evolution of 3D printed soft actuators," *Sens. Actuators A, Phys.*, vol. 250, pp. 258–272, Oct. 2016.
[29] J. Z. Gul, M. Sajid, M. M. Rehman, G. U. Siddiqui, I. Shah, K. H. Kim, J. W. Lee, and K. H. Choi, "3D printing for soft robotics–a review," *Sci. Technol. Adv. Mater.*, vol. 19, no. 1, pp. 243–262, 2018.
[30] Y. Li, Y. Chen, Y. Yang, and Y. Wei, "Passive particle jamming and its stiffening of soft robotic grippers," *IEEE Trans. Robot.*, vol. 33, no. 2, pp. 446–455, Apr. 2017.
[31] R. Pfeifer, M. Lungarella, and F. Iida, "The challenges ahead for bio-inspired 'soft' robotics," *Commun. ACM*, vol. 55, no. 11, pp. 76–87, Nov. 2012.
[32] Wikipedia. *Hand*. [Online]. Available: https://en.wikipedia.org/wiki/Hand
[33] V. Trappe, V. Prasad, L. Cipelletti, P. N. Segre, and D. A. Weitz, "Jamming phase diagram for attractive particles," *Nature*, vol. 411, no. 6839, pp. 772–775, Jun. 2001.
[34] P. Polygerinos, Z. Wang, J. T. Overvelde, K. C. Galloway, R. J. Wood, K. Bertoldi, and C. J. Walsh, "Modeling of soft fiber-reinforced bending actuators," *IEEE Trans. Robot.*, vol. 31, no. 3, pp. 778–789, Jun. 2015.
[35] G. Gerboni, A. Diodato, G. Ciuti, M. Cianchetti, and A. Menciassi, "Feedback control of soft robot actuators via commercial flex bend sensors," *IEEE/ASME Trans. Mechatronics*, vol. 22, no. 4, pp. 1881–1888, Aug. 2017.
[36] S. H. Foulger, "Electrical properties of composites in the vicinity of the percolation threshold," *J. Appl. Polym. Sci.*, vol. 72, no. 12, pp. 1573–1582, Jun. 1999.
[37] E. Segal, R. Tchoudakov, M. Narkis, and A. Siegmann, "Thermoplastic polyurethane-carbon black compounds: Structure, electrical conductivity and sensing of liquids," *Polym. Eng. Sci.*, vol. 42, no. 12, pp. 2430–2439, Dec. 2002.
[38] Y. Yang and Y. Chen, "Innovative design of embedded pressure and position sensors for soft actuators," *IEEE Robot. Autom. Lett.*, vol. 3, no. 2, pp. 656–663, Apr. 2018.
[39] *PI-ETPU Filament*. [Online]. Available: https://www.creativetools.se/hardware/3d-printers-and-accessories/filaments/flexible-filaments/pi-etpu-95-250-carbon-black
[40] *NinjaFlex Flexible Filament*. [Online]. Available: https://ninjatek.com/ninjaflex/
[41] H. K. Yap, H. Y. Ng, and C.-H. Yeow, "High-force soft printable pneumatics for soft robotic applications," *Soft Robot.*, vol. 3, no. 3, pp. 144–158, Sep. 2016.
[42] Y. Li, Y. Chen, T. Ren, and Y. Hu, "Passive and active particle damping in soft robotic actuators *this work is funded by a basic research grant from the University of Hong Kong," in *Proc. IEEE Int. Conf. Robot. Automat. (ICRA)*, May 2018, pp. 1547–1552.

YANG YANG (Member, IEEE) received the B.S. degree in mechanical design manufacturing and automation and the M.S. degree in mechatronics engineering from the Harbin Institute of Technology, China, in 2011 and 2013, respectively, and the Ph.D. degree in mechanical engineering from The University of Hong Kong, Hong Kong, in 2017.

Before joining the Nanjing University of Information Science and Technology, Nanjing, China, as a University Hired Professor, in 2020, he has worked as a Postdoctoral Fellow with The University of Hong Kong and The Hong Kong University of Science and Technology, from 2017 to 2020. His research interests include soft robots, bio-inspired robots, 3D Printing, and smart materials.

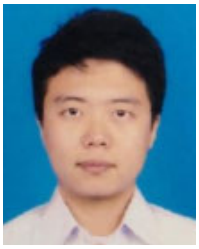

YUNQUAN LI (Member, IEEE) received the B.S. degree in mechanical engineering and automation from the South China University of Technology, China, in 2014, and the M.Sc. degree from the Department of Mechanical Engineering, The University of Hong Kong, in 2015. He is currently pursuing the Ph.D. degree in mechanical engineering with The University of Hong Kong.

His research interests include soft robotics, compliant mechanisms, mechanical systems, and robotic design.

YONGHUA CHEN (Member, IEEE) received the B.Sc. degree in mechanical engineering from Southwest Jiaotong University, Chengdu, China, in 1985, and the Ph.D. degree in mechanical engineering from the University of Liverpool, Liverpool, U.K., in 1990.

Before joining The University of Hong Kong, as a Lecturer, he had been with Motorola Electronics Pte, Ltd., Singapore, Asia Matsushita Electronics Pte, Ltd., Singapore, and Swire Technologies Pte, Ltd., Hong Kong, where he had acquired experience in automation, robotics, and engineering design. He is currently an Associate Professor with the Department of Mechanical Engineering, The University of Hong Kong. He has filed one patent, coauthored a book, and published more than 160 refereed articles in international journals and conferences. His research interests include service robotics, smart soft robotics, and additive manufacturing.

YINGTIAN LI (Member, IEEE) received the B.Sc. degree in material forming and control engineering from Tianjin University, China, in 2012, and the M.Sc. and Ph.D. degrees in mechanical engineering from The University of Hong Kong, in 2013 and 2018, respectively.

He is currently an Associate Professor with the Shenzhen Institute of Advanced Technology, Chinese Academy of Sciences, Shenzhen, China. His research interests include soft robotics, compliant robotics, continuum robotics, and hyper redundant robotics.

TAO REN received the B.S. degree in process equipment and control engineering, the M.S. degree in power engineering, and the Ph.D. degree in mechanical engineering from Southwest Petroleum University, Chengdu, China, in 2011, 2014, and 2017, respectively.

From 2015 to 2016, he was a Research Associate with the Department of Mechanical Engineering, The University of Hong Kong. He is currently with the College of Nuclear Technology and Automation Engineering, Chengdu University of Technology, China. His research interests include design, modeling, and control of advanced mechatronics systems.

YI REN received the bachelor's degree in thermal energy and power engineering and the M.Sc. and Ph.D. degrees in mechatronic engineering from the Harbin Institute of Technology, Harbin, China, in 2011, 2013, and 2017, respectively.

Since 2018, he has been working as a Postdoctoral Researcher of electrical engineering with the Chair of Information-Oriented Control, Department of Electrical and Computer Engineering, Technical University of Munich, Munich, Germany. Since 2020, he has also been a Research Scientist with Robotics X Lab, Tencent. His research interests include robotics, nonlinear control, human–multirobot interaction, and distributed control with application to multirobot cooperation and manipulation.